Effects of Boundary-Layer Ingestion on the Aero-Acoustics of Transonic Fan Rotors

Jeffrey J. Defoe[1]

Zoltán S. Spakovszky

Gas Turbine Laboratory,
Massachusetts Institute of Technology,
Cambridge, MA 02139

The use of boundary-layer-ingesting, embedded propulsion systems can result in inlet flow distortions where the interaction of the boundary-layer vorticity and the inlet lip causes horseshoe vortex formation and the ingestion of streamwise vortices into the inlet. A previously-developed body-force-based fan modeling approach was used to assess the change in fan rotor shock noise generation and propagation in a boundary-layer-ingesting, serpentine inlet. This approach is employed here in a parametric study to assess the effects of inlet geometry parameters (offset-to-diameter ratio and downstream-to-upstream area ratio) on flow distortion and rotor shock noise. Mechanisms related to the vortical inlet structures were found to govern changes in the rotor shock noise generation and propagation. The vortex whose circulation is in the opposite direction to the fan rotation (counter-swirling vortex) increases incidence angles on the fan blades near the tip, enhancing noise generation. The vortex with circulation in the direction of fan rotation (co-swirling vortex) creates a region of subsonic relative flow near the blade tip radius that decreases the sound power propagated to the far-field. The parametric study revealed that the overall sound power level at the fan leading edge is set by the ingested streamwise circulation, and that for inlet designs in which the streamwise vortices are displaced away from the duct wall, the sound power at the upstream inlet plane increased by as much as 9 dB. By comparing the far-field noise results obtained to those for a conventional inlet, it is deduced that the changes in rotor shock noise are predominantly due to the ingestion of streamwise vorticity. [DOI: 10.1115/1.4023461]

1 Introduction

Fan rotors with supersonic relative flow at the blade tips generate rotor shock noise that propagates upstream through the inlet to the far-field. In nonuniform flow, the generated shocks have varying strengths and propagation directions. They therefore interact as they propagate upstream, leading to a pressure field with once-per-revolution periodicity. This paper presents the results of an investigation into the effects of serpentine inlet duct geometry on the generation and propagation of rotor shock noise in boundary-layer-ingesting propulsion systems.

Prior work in the literature on the numerical prediction of rotor shock noise has focused on uniform flows and conventional, axisymmetric inlets. The one-dimensional model by Mathews and Nagel [1] provided approximate predictions of shock decay rates in axisymmetric inlets, neglecting three-dimensional flow effects. Prasad and Feng [2] computed the propagation of upstream-traveling waves in a conventional inlet. The axisymmetric geometry allowed a steady computation to be carried out in the fan reference frame, greatly reducing computational cost. 3D flow effects were assessed by examining two inlets that varied only in their throat areas. The authors discovered that increased local flow accelerations near the nacelle in the inlet with reduced throat area enhanced noise attenuation.

The detailed study of flow through serpentine inlets with boundary-layer ingestion (BLI) was studied by Plas et al. [3] and Madani and Hynes [4]. Plas et al. conducted a parametric study of serpentine duct designs to determine the effects of duct geometry (offset ratio and area ratio) on the flow distortion at the downstream end of the duct as characterized by the pressure recovery and the $DC(60)$ distortion coefficient. All computations were conducted at cruise conditions. The results are useful for placing bounds on what parameter space describing serpentine ducts leads to acceptable levels of distortion at the fan. Madani and Hynes considered the effect of the duct contour on the downstream distortion. Starting from the best case with minimum fan face distortion from Ref. [3], the duct contour was optimized for low fan face flow distortion. The optimized duct showed some improvement but the change in flow distortion was small compared to changes due to duct offset and area ratio. It was concluded that duct geometry parameters such as the offset and area ratios have a stronger effect on the distortion transfer characteristics than the details of the serpentine duct contour.

Sound propagation in nonuniform flow is a challenging problem. General expressions for sound intensity, useful in any computed flow, were derived by Myers [5]. In this approach, linear waves need not be assumed. Brambley and Peake [6,7] investigated the propagation of linear acoustic waves through circular and annular ducts with radii of curvature comparable to the duct diameter and where the duct length to diameter ratio is large. The approach assumed potential flow and linear waves. The key result was that cut-on/cut-off criteria were not significantly altered from the straight-duct values for the potential duct flow considered.

In order to investigate the propagation of rotor shock noise through boundary-layer ingesting inlets, in which the duct flow is rotational, a new approach must be developed. In addition, the duct aerodynamics at low flight speed must be assessed as this is relevant to community noise.

A methodology capable of generating and propagating rotor shock noise in nonuniform flow has recently been developed and applied to a conventional inlet-fan system [8] and a single serpentine inlet system [9]. The latter study revealed that for the serpentine inlet, the source sound power was increased by 38 dB near the fan face and tones in the far-field above one-half of the blade-passing frequency were attenuated below the noise floor. The same methodology is applied here to a parametric study of serpentine inlet ducts.

[1]Currently MHI Senior Research Fellow and Girton College Lecturer at the Whittle Laboratory, University of Cambridge.

Contributed by the International Gas Turbine Institute (IGTI) of ASME for publication in the JOURNAL OF TURBOMACHINERY. Manuscript received July 15, 2012; final manuscript received November 2, 2012; published online June 26, 2013. Editor: David Wisler.

2 Scope of the Paper

The objectives of this paper are: (1) to determine the mechanisms by which rotor shock noise is altered as a result of boundary-layer ingestion, and (2) to quantify how serpentine inlet duct geometry affects the rotor shock noise.

The approach is to parametrically vary the serpentine inlet geometry, holding fixed the ingested boundary-layer properties, fan corrected flow, and free-stream Mach number. An overview of the modeling approach, the parameter space for the serpentine inlets, and the setup of the airframe-engine integration are presented next. This is followed by an overview of the computational setup. It will then be shown that the overall sound power level at the fan leading edge is set by the ingested streamwise circulation, and for inlet designs in which the streamwise vortices are displaced away from the duct wall, the sound power at the upstream inlet plane increased by as much as 9 dB. By comparing the far-field noise results to those previously obtained for a conventional inlet, it is deduced that the changes in rotor shock noise are predominantly due to the ingestion of streamwise vorticity.

In light of these findings, the paper addresses the following research questions in detail: (1) what is the mechanism leading to enhanced sound power generation with boundary-layer ingestion, (2) what mechanisms in the flow contribute to changes in in-duct sound propagation, and (3) how do changes in the flow owing to altered duct geometry affect rotor shock noise generation and propagation?

3 Modeling Approach

The key idea is to represent the fan rotor with a rotating body force field that generates rotor shock noise; its time-mean component provides the quasi-steady pressure rise and flow turning of the rotor. A single-passage, steady 3D Reynolds-averaged Navier–Stokes (RANS) calculation of the fan rotor is first carried out to obtain the body-force-based description of the blade row performance. The body force field description thus obtained can respond locally to the flow conditions such that the effects of inlet distortion are captured. The body force field is then perturbed by a rotor-locked disturbance to create rotor shock noise. This perturbation, its shape derived from the 3D RANS calculation, is periodic over one blade pitch and generates the blade leading edge shock and expansion fan system. The body force formulation is then implemented in a full-domain unsteady Euler calculation and the far-field noise is determined via the Ffowcs–Williams and Hawkings (FW-H) integral method using a permeable surface. A more detailed description and validation of this approach using 3D computational fluid dynamics (CFD) calculations and experimental data for the same fan studied here can be found in Ref. [8].

In this paper, the body force approach is implemented for serpentine inlets in an integrated propulsion system configuration with boundary-layer ingestion. For all inlets, the same NASA/GE R4 rotor with 22 rotor blades was considered at the cutback operating condition (87.5% corrected design speed). The fan exit guide vanes were not included in this analysis although the methodology could be extended in the future to capture blade-row interaction noise. The fan exhaust was ducted out of the computational domain to prevent fan exhaust noise from contributing to the far-field noise levels.

3.1 Duct Geometry Parameters and Computational Setup. Figure 1 depicts the four inlets analyzed. The parameters varied in this investigation are the duct area ratio and offset ratio, defined as $AR = A_{AIP}/A_{throat}$ and $OR = \delta/D_{AIP}$, respectively. A_{throat} and A_{AIP} are the areas of the upstream and downstream ends of the serpentine duct; δ is the vertical duct offset and D_{AIP} is the downstream duct diameter. The ducts have circular cross sections over their entire lengths. The four cases are $AR = 1.01$ and 1.05 and $OR = 0.25$ and 0.75. All ducts have axial length-to-diameter ratios $L/D_{AIP} = 2$. The limits on area ratio were chosen to be

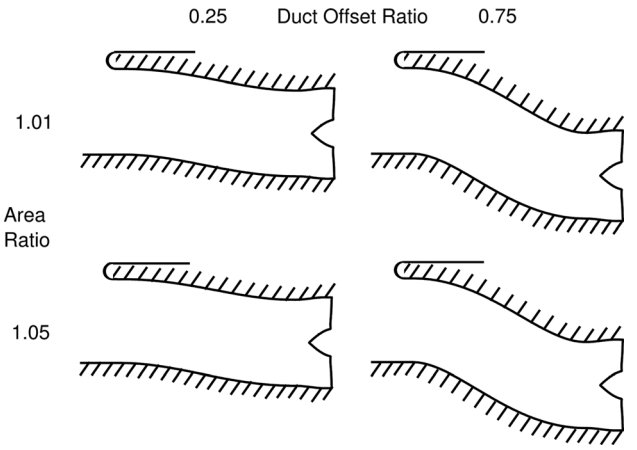

Fig. 1 Serpentine inlets used in the parametric study

consistent with the work of Madani and Hynes [4] and are representative of a typical inlet for an embedded propulsion system in a hybrid wing-body aircraft configuration. While including an $OR = 0$ configuration would have been desirable, time limited the parametric study to two nonzero offsets. For the conditions investigated here, two-dimensional viscous calculations have shown that the in-duct flow separates at offset ratios approaching 1.0 and the highest offset ratio of 0.75 was selected to ensure that the serpentine inlet flow remains attached.

The duct geometries consist of cosine centerline distributions with linearly varying areas. The centerlines are given by

$$\frac{y}{D} = \frac{OR}{2}\left(1 + \cos\left(\pi\left[2\frac{x}{D} - 1\right]\right)\right) \tag{1}$$

and the cross-sectional areas are given by

$$A^* = \frac{1}{AR} + \left(1 - \frac{1}{AR}\right)\frac{s^*}{s^*_{max}} \tag{2}$$

where A^* is the duct area normalized by the aerodynamic interface plane (AIP) area, and s^* is the dimensionless arc length along the duct centerline.

The serpentine inlet ducts are mated to the diffusing portion of the NASA/GE R4 conventional inlet described in Ref. [10] such that the AIP, defined as the furthest upstream location where the duct axis centerline is coincident with the fan axis, is located at the throat of the conventional inlet as illustrated in the inset of Fig. 2. At the upstream end, the serpentine inlets are flush-mounted on a flat plate representing an airframe upper surface, with the circular inlet smoothly blended (C^1 continuous) with the plate. A flat plate is used since the focus is on the acoustics rather than the external aerodynamics, but the boundary-layer thickness in the calculation is representative of that of a hybrid wing-body airframe centerbody.

The computational domain includes the rotor region, the upstream duct and inlet, and the external flow field, as illustrated in Fig. 2. The suction surface boundary layer and related stagnation pressure deficit are defined 10 diameters upstream of the inlet using previously conducted viscous 3D airframe computations [11]. The inherent numerical dissipation present in the inviscid solver is compensated for using the technique presented previously in Ref. [9]. The FW-H surface is placed approximately 1.5 fan diameters from the inlet throat where the average pressure coefficient (normalized by the free-stream dynamic pressure) is less than 1% of the pressure coefficient at the duct inlet. The serpentine inlet domains contain approximately 15×10^6 cells in a structured grid topology. Variation in cells sizes in the rotor region, inlet duct, and in the near-field region up to the FW-H

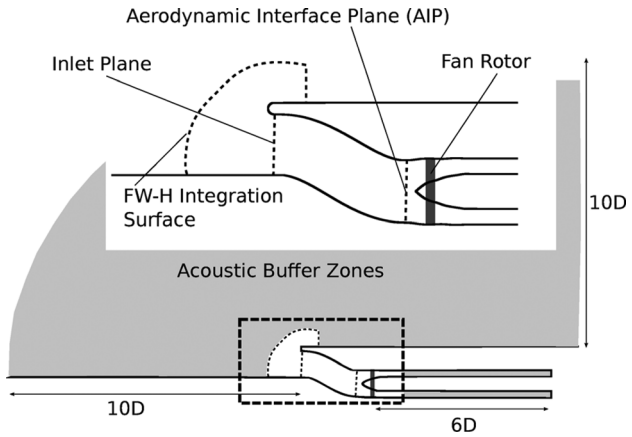

Fig. 2 Schematic illustration of computational domain and key data plane locations

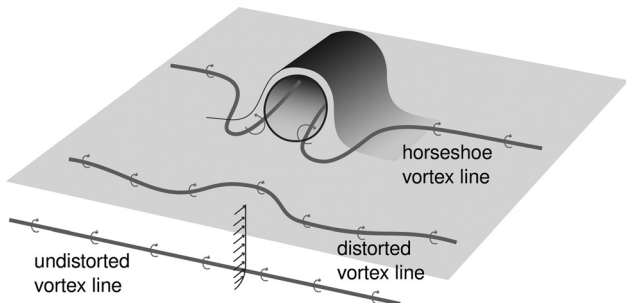

Fig. 3 Generation and ingestion of streamwise vorticity due to boundary-layer ingestion

surface are minimized to reduce numerical dispersion. The cell size is based on a wave resolution of 25 points per wavelength for the shortest wavelength of interest (blade-passing). The time step was chosen to be 1/60 of a blade-passing period. These cell and time step sizes were chosen based on the results of a parametric study of solver behavior [12] and are consistent with findings in the literature for second-order accurate finite-volute CFD codes [13,14]. Acoustic buffer zones are placed outside the FW-H surface and in the duct far downstream of the rotor to prevent spurious wave reflections. The buffer zone formulation uses grid stretching and explicit damping [15]. The corrected flow through the inlet is set to the cut-back value of 83% of design for the R4 fan rotor. The free-stream Mach number is 0.1, representative of near-takeoff conditions.

4 Mean Flow Aerodynamic Results

Two features of the duct mean flow aerodynamics that play an important role in rotor shock noise generation and propagation are the ingestion of streamwise vorticity and, for the duct with $AR = 1.01$ and $OR = 0.75$, the in-duct lift-off of the streamwise vortices. These phenomena are discussed next.

4.1 Ingestion of Streamwise Vorticity. At a cruise Mach number of 0.8 the ingested boundary layer occupies approximately 30% of the inlet height [4] with an inlet pressure recovery at the AIP of approximately 0.92 of the free-stream stagnation pressure. At the low-speed condition considered here, $M_\infty = 0.1$, there is approximately 20% BLI and the inlet pressure recovery is equal to 0.99. In both cases the AIP Mach number is approximately 0.5, so that the flow decelerates into the inlet at cruise and accelerates into the inlet at the low-speed condition. Thus, at low speeds the ingested vorticity in the boundary layer is more

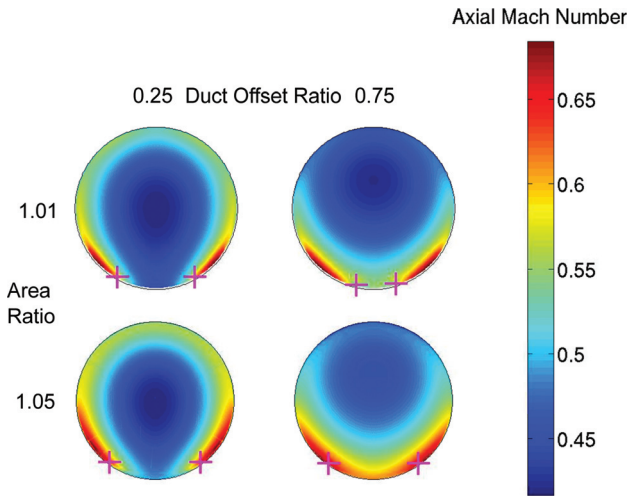

Fig. 4 Localized flow accelerations in axial Mach number at the inlet plane. Magenta crosses indicate locations of vortex cores.

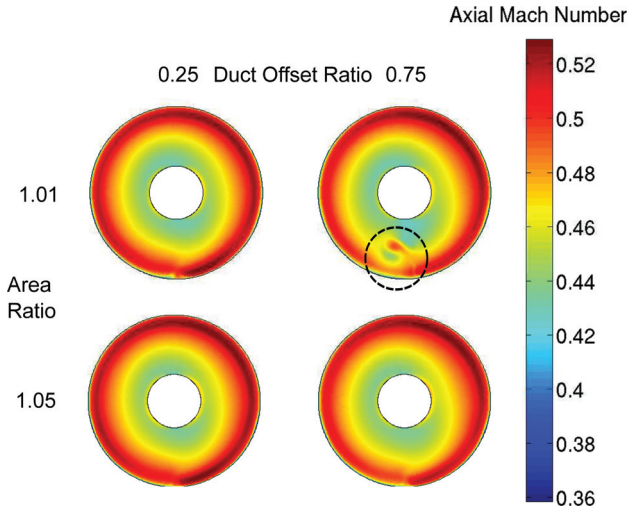

Fig. 5 Axial Mach number at the fan leading edge, showing vortex lift-off for the duct with $AR = 1.01$ and $OR = 0.75$

important than the stagnation pressure deficit. While this vorticity is perpendicular to the flow direction well upstream of the inlet, as it interacts with the inlet lip it is tipped into and stretched along the streamwise direction as depicted in Fig. 3. The streamwise vorticity is enhanced by the stretching of the vortex lines as the flow accelerates into the inlet. The result is the creation of regions of high-speed flow centered around the vortex cores. This phenomenon occurs at the inlet planes of all the inlet ducts considered, as shown by the axial Mach number contours in Fig. 4. The magenta crosses indicate the estimated locations of the vortex cores.

Each duct's vortices are of a different size and the locations of the vortex cores are similar except for the duct with $AR = 1.01$ and $OR = 0.75$, for which they are closer together. The behavior of this duct is qualitatively different than the other three in that the streamwise vortices lift off the duct bottom in the inlet, as can be seen at the fan leading edge in Fig. 5. The consequences of this are investigated next.

4.2 Vortex Lift-Off. A combination of the local flow acceleration at the upstream end of the duct and the large normal pressure gradients is responsible for vortex lift-off in the $AR = 1.01$

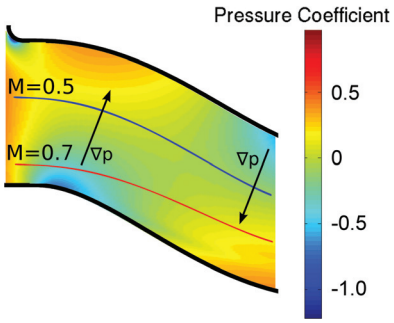

Fig. 6 Pressure coefficient on duct symmetry plane for *AR* = 1.01, *OR* = 0.75 case, schematically depicting the effects of vortex lift-off

Table 1 Vortex core axial Mach numbers on inlet planes. Departures from mass-averaged Mach numbers are given in parentheses.

AR \ *OR*	0.25	0.75
1.01	0.62 (+0.13)	0.70 (+0.21)
1.05	0.61 (+0.10)	0.68 (+0.17)

and $OR = 0.75$ duct case. Counterrotating vortex pairs produce an induced velocity field that results in the vortices being set in motion [16]. For the inlets under consideration, this induced velocity is negligible since it is approximately two orders of magnitude smaller than the mean duct velocity based on the inlet diameter and corrected flow. This allows the use of simple momentum arguments to describe the vortex lift-off phenomenon. Considering the steady momentum equation normal to the flow direction for inviscid flow

$$\frac{\partial p}{\partial n} = -\frac{\rho u^2}{r_c} \tag{3}$$

where r_c is the local radius of curvature, the higher-velocity flow near the vortex cores will have a larger radius of curvature when subjected to the same pressure gradient across the duct than will the surrounding lower-velocity flow. This results in the upward displacement of the vortex core streamlines. The amount of displacement depends on two factors: the magnitude of the normal pressure gradient (which itself depends on the duct offset) and the ratio of the vortex core velocity to the mean duct velocity.

The vortex core lift-off is shown in Fig. 6, which depicts the pressure coefficient on the duct symmetry plane for the $AR = 1.01$, $OR = 0.75$ inlet. The change in area ratio has only a modest effect on the mass-averaged Mach number at the upstream end of the duct (0.49 for $AR = 1.01$ and 0.51 for $AR = 1.05$) such that the duct offset ratio is the primary factor that affects the vortex line stretching and, thus, the peak axial Mach number. The vortex core axial Mach numbers on the inlet planes and respective departures from the mass-averaged Mach numbers are summarized in Table 1. The highest vortex core axial Mach number, combined with the lower mass-averaged Mach number for the $AR = 1.01$ ducts and larger normal pressure gradients present in the $OR = 0.75$ ducts, is responsible for the lift-off of the streamwise vortices. In the other ducts the pressure gradient and/or the ratio of vortex core axial Mach number to mass-averaged Mach number on the inlet plane are not sufficient to produce a visible lift-off of the streamwise vortices.

4.3 Fan Aerodynamics. The effects of the ingested streamwise vorticity on the flow at the AIP and fan leading edge are assessed to determine their impact on the fan performance. The three ducts without vortex lift-off have similar distortions at the AIP and fan, with vorticity-induced distortions in the outer span. In contrast, in the $AR = 1.01$, $OR = 0.75$ duct the streamwise vorticity is concentrated near midspan. The consequences of this change are explored next.

Table 2 *DC* (60) at AIP and fan leading edge for parametric study

Duct	AIP	Fan leading edge
$AR = 1.01$, $OR = 0.25$	0.009	0.008
$AR = 1.01$, $OR = 0.75$	0.017	0.013
$AR = 1.05$, $OR = 0.25$	0.006	0.004
$AR = 1.05$, $OR = 0.75$	0.007	0.004

A common metric for quantifying the degree of inlet distortion is the $DC(60)$ distortion descriptor, defined as

$$DC(60) = \frac{\bar{p}_t^{\mathrm{M}} - \bar{p}_{t,\,\text{avg. over worst 60 deg}}^{\mathrm{M}}}{\overline{p_t} - \overline{p}^{\mathrm{M}}}. \tag{4}$$

For inlet distortion at cruise conditions, Madani and Hynes [4] reported $DC(60)$ values at AIP ranging from 0.414 to 0.625 depending on the duct geometry. Table 2 lists the computed $DC(60)$ values at AIP and fan leading edge for the current study. While the duct with lifted-off streamwise vortices has $DC(60)$ values approximately two to three times higher than those of the other ducts, all the values in the table are at least an order of magnitude smaller than at cruise. This indicates that $DC(60)$ is not the appropriate metric for this distortion, which is due to the presence of streamwise vorticity rather than the stagnation pressure deficit at low-speed free-stream conditions.

The vortices alter the local operating points of the fan blade row by changing the incoming relative Mach number, as depicted at the outer radius in Fig. 7. On the abscissa 0 degrees marks the location of the bottom center of the duct. The regions of subsonic and enhanced supersonic relative flow near the duct bottom (between −50 deg and 50 deg) are due to the streamwise vortices. The impact of the vortices on the relative Mach number is also given schematically in the figure. The variations in the relative Mach number in the remainder of the circumference are due to the redistribution of flow caused by the streamwise vortices. The duct in which the vortex lift-off phenomenon occurs (shown in blue) does not exhibit a strong increase in relative Mach number between 0 deg and 50 deg because of the displacement of the counter-rotating vortex away from the end wall.

5 Acoustic Results

The source noise is affected by duct geometry through the interaction with ingested streamwise circulation that determines the change in source strength relative to clean, axisymmetric inlet flow. As will be shown, the in-duct sound power attenuation is reduced by 9 dB relative to the other inlets considered as a result of lifted-off streamwise vortices as the counter-swirling vortex decreases the attenuation rate of cut-off waves near midspan. The changes in far-field spectra are predominantly due to a combination of in-duct attenuation for short wavelengths and the effect of nonuniform external flow on sound radiation.

5.1 Noise Source Generation. The rotor shocks are generated just upstream of the fan leading edge but noise is generated throughout the upstream region of shock interaction due to the nonuniform flow. The changes in the source noise resulting from vortex lift-off can be seen by comparing the plots of Fig. 8, which depicts unwrapped instantaneous contours of relative Mach number at 92% span between the fan leading edge and AIP for cases $AR = 1.05$ and $OR = 0.75$ (no vortex lift-off) and $AR = 1.01$ and

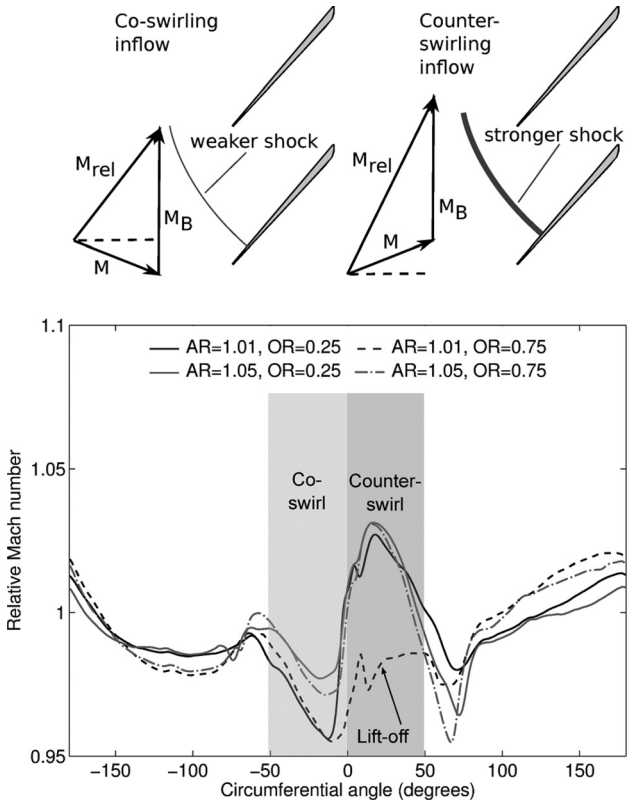

Fig. 7 Relative Mach number versus circumferential angle at outer radius (casing) as influenced by co- and counter-swirl. Top: effect of co- and counter-swirl on shock strength and location.

$OR = 0.75$ with vortex lift-off. Vortex lift-off spreads out the effect of the co-rotating vortex at 92% span since the vortex core is situated near midspan. While the shock structure near the fan is weakly altered by vortex lift-off, the upstream propagation is changed due to the differences in the flow field in the outer span.

5.2 In-Duct Propagation. There are two distinct cases to consider depending on the location of the streamwise vortices: the vortices can either be localized in the outer span or can be shifted towards the duct centerline by vortex lift-off. The former case primarily alters the sound power by attenuating high frequencies, while this effect is reduced when the distortion is concentrated near midspan.

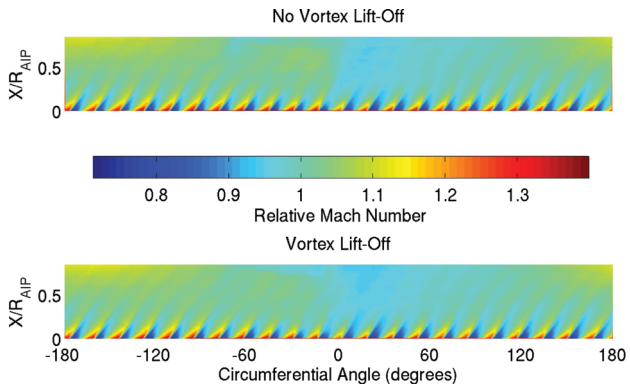

Fig. 8 Relative Mach number at 92% span between fan leading edge and AIP. Top: $AR = 1.05$ and $OR = 0.75$ case without vortex lift-off. Bottom: $AR = 1.01$ and $OR = 0.75$ case with vortex lift-off.

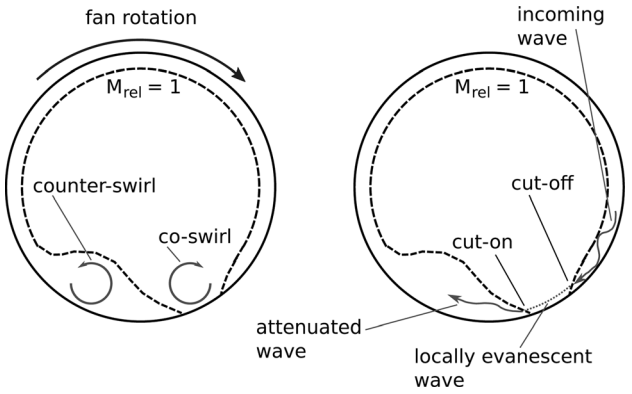

Fig. 9 Wave attenuation by co-swirling streamwise vortex in the outer span

First, consider streamwise vortices located in the outer span, as illustrated on the left in Fig. 9. The key mechanism responsible for altering the in-duct propagation (relative to uniform inflow) is the creation of a region of evanescent wave behavior by the co-swirling vortex as the relative Mach number is reduced below sonic conditions. When waves pass through this region they decay in amplitude as illustrated in the right part of Fig. 9. The result is enhanced duct power attenuation compared to the undistorted inflow case. This mechanism affects wavelengths on the order of the extent of the subsonic relative flow region more strongly than wavelengths on the order of the circumference.

Next, consider streamwise vortices lifted off the duct wall, depicted in Fig. 10. The counter-swirling vortex increases the local relative Mach number near midspan such that waves passing through this region have reduced decay rates. This effect will also be more pronounced for short wavelengths (higher frequencies) similarly to the other case. The consequence of waves spiraling upstream through the inlet with vortex lift-off is the reduced decay of the sound power as shown in Fig. 11. The decay from AIP to inlet plane for this case is 15 dB whereas on average the decay for the other three ducts is 22 dB, resulting in a 7 dB higher sound power propagated through the serpentine portion of the inlet.

To further investigate the reduced sound power decay around the lifted-off counter-swirling vortex, the overall sound intensity fields are computed at AIP and the duct inlet plane following the methodology for acoustic energy developed by Myers [5]. This general approach is required in the presence of nonuniform flow, as modal decompositions of the acoustic field based on analytical solutions to the wave equation apply only to uniform flows.

In Fig. 12 on the left, local intensity enhancement of 20 dB to 30 dB is observed for the case with vortex lift-off ($AR = 1.01$ and $OR = 0.75$). As the streamwise vortices shift towards the outer

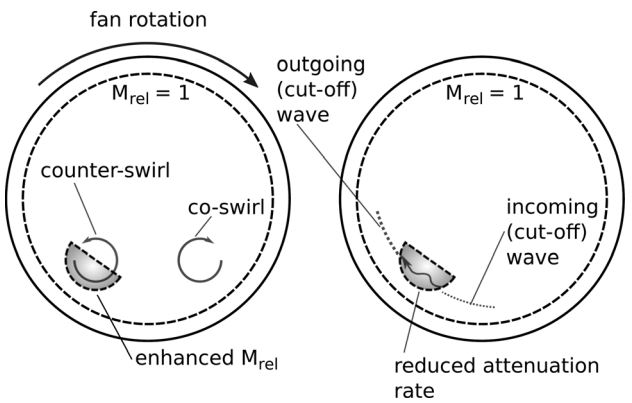

Fig. 10 Reduction in sound power decay rate due to counter-swirling, lifted-off streamwise vortex

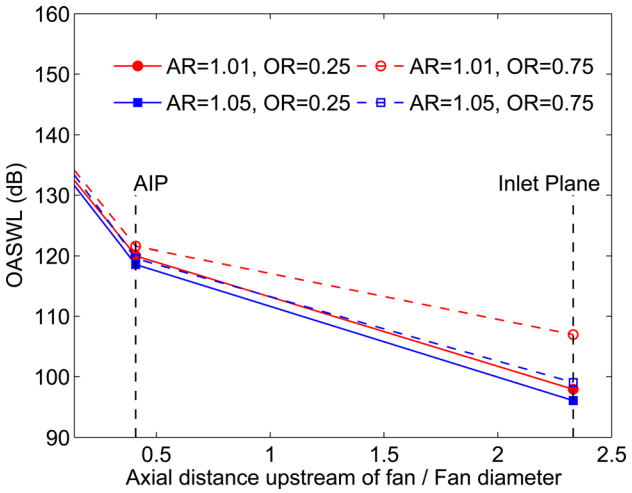

Fig. 11 In-duct overall sound power level (up to and including the blade-passing frequency) evolution, showing the enhancement in sound power resulting from vortex lift-off (blue line)

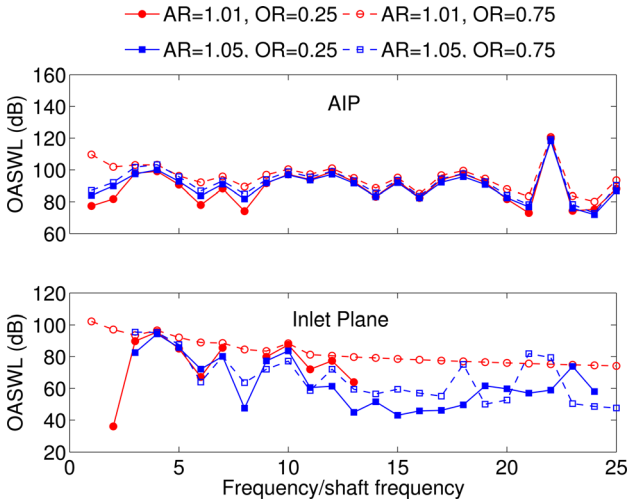

Fig. 13 Sound power spectra at the AIP and inlet plane, showing the decay of the BPF ($f/f_{shaft} = 22$) tone. Missing data points indicate that no upstream-propagating sound power is present at that frequency.

duct radius at the inlet plane, the enhanced sound intensity region migrates as well, as seen in Fig. 12 on the right.

As can be seen in the spectra of Fig. 13, the frequencies most affected by the vortex lift-off are those between one-half blade-passing frequency (BPF) and BPF, 11 and 22 times the shaft frequency. In particular, the spectra at the inlet plane show increased attenuation of the high-frequency tones, particularly the blade-passing tone. For the duct with vortex lift-off, $AR = 1.01$ and $OR = 0.75$, the 9 dB increase in overall sound power is concentrated at frequencies of 13 to 20 times the shaft frequency.

5.3 Far-Field Propagation. The full-scale sound pressure level spectra were computed four duct diameters from the fan axis to quantify the far-field noise. The spectra in Fig. 14 share the common characteristic of an apparent cut-off of tones above approximately one-half of the BPF, which is not affected by the duct geometry. However, the inlets with area ratios of 1.05 have higher noise floors than the inlets with area ratios of 1.01, which may be related to the increased flow nonuniformities outside the inlet for the $AR = 1.05$ ducts; the underlying mechanism is not yet fully understood. It was hypothesized that spherical spreading effects might account for the attenuation of the blade-passing tone. However, an investigation showed that the apparent cut-off in the far-field is not an artifact of levels falling below the numerical noise floor, as the attenuation due to spherical spreading is insufficient to produce such a result: at the FW-H surface, the BPF tone is only attenuated by 0.25 dB more than the fan shaft frequency.

The 9 dB enhancement in sound power at the inlet plane for the $AR = 1.01$, $OR = 0.75$ duct is not evident in the far-field because the additional acoustic energy at the inlet plane is concentrated at frequencies above one-half of the blade-passing frequency. The conjecture is that the nonuniform flow outside the duct is responsible for the cut-off of the high-frequency tones, including the blade-passing frequency. Since this external flow is largely unchanged throughout the parametric study, it follows that there is no significant change in the far-field apparent cut-off frequency between the various ducts. To establish the link between the external flow and the far-field cut-off frequency, computations in which the stagnation point on the nacelle is varied need be carried out. This is to be investigated in future work.

5.4 Comparison—Conventional Inlet Rotor Shock Noise. The changes in far-field noise relative to previously obtained, validated results for a conventional inlet with no flow distortion [8] are analyzed to determine the effects of duct geometry on the peak far-field levels and directivity. In summary, the

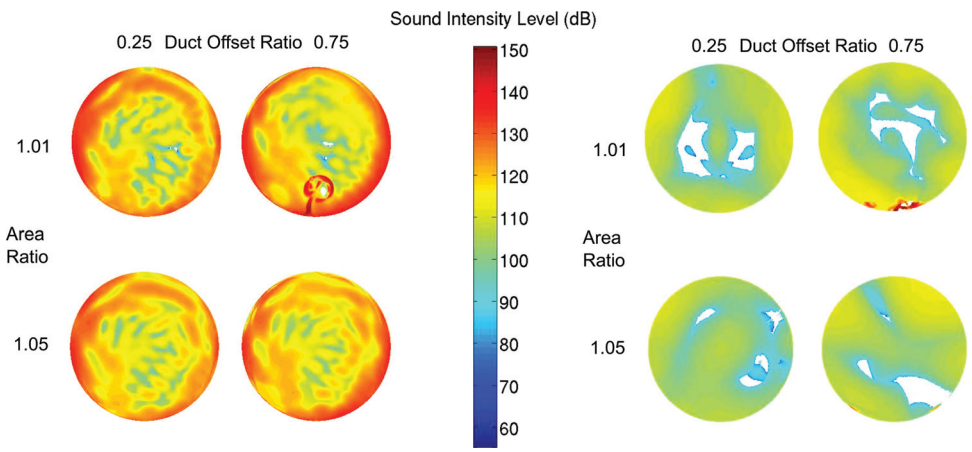

Fig. 12 Overall sound intensity fields (up to and including the blade-passing frequency) at AIP (left) and duct inlet plane (right). Propagation of sound power is increased due to the lifted-off counter-swirling streamwise vortex.

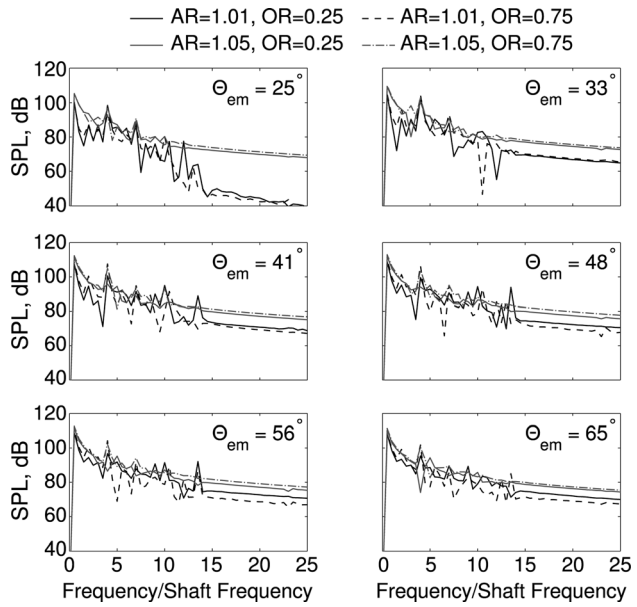

Fig. 14 Far-field spectra at various emission angles Θ_{em}; BPF is equal to $f/f_{shaft} = 22$

Table 3 Peak change in OASPL (in dB) relative to conventional inlet

AR \ *OR*	0.25	0.75
1.01	13.2	14.2
1.05	17.1	17.9

peak overall sound pressure level (OASPL) is increased between 13 dB and 18 dB for the four inlets considered, with 4 dB of this 5 dB range attributed to the change in area ratio as a result of changes in the external flow. The increases in peak level are given in Table 3. Since the corrected flow through the inlets is the same for all ducts, the peak axial Mach numbers on the inlet plane increase with *AR*, increasing the relative Mach number that enhances propagation and the far-field noise levels.

5.5 Preliminary Design Guidelines. Based on the findings from the parametric study, the following preliminary design guidelines for low-noise embedded propulsion systems can be stated:

- For inlets with offset ratios as high as 0.75, the AIP to inlet plane area ratio must be greater than 1.01 to avoid vortex lift-off.
- Since increasing *AR* from 1.01 to 1.05 increases the far-field noise by 4 dB on average, using a large *AR* to eliminate vortex lift-off will not reduce far-field noise. Over the range of flows and duct parameters investigated, flow distortion due to streamwise vortices always increases far-field noise. Furthermore, the increase in far-field noise of at least 13 dB is much larger than the 5 dB maximum variation observed as a result of changes in inlet geometry.
- Shaping the inlet lip geometry, such as by using leading edge strake extensions, can mitigate streamwise vorticity development.

The first two items above suggest that, to minimize rotor shock noise propagation in the presence of BLI, both the area ratio and offset ratio of the duct should be minimized. In many applications, however, this may not be possible due to other design trade-offs. It might also be possible to take advantage of the shift in acoustic energy towards low frequencies to enhance the effectiveness of acoustic liners in the inlet duct.

6 Conclusions and Outlook

The dominant mechanism for changes in far-field rotor shock noise due to boundary-layer ingestion at low flight speeds is the ingestion of streamwise vorticity. The *DC*(60) distortion descriptor is, thus, not an appropriate metric for quantifying flow distortion under these conditions. Specific conclusions that apply to the fan rotor and inlet geometries considered in this study are:

- Boundary-layer ingestion at low speed ($M_\infty = 0.1$) increases source sound power up to 38 dB for the NASA/GE R4 fan rotor but only increases far-field overall sound pressure levels by 18 dB. The additional sound power attenuation in the inlet duct is due to locally evanescent wave behavior where the co-swirling streamwise vortex lowers the relative Mach number below the sonic point.
- Lift-off of the streamwise vortices from the duct bottom occurs for the high offset ($OR = 0.75$), low area ratio ($AR = 1.01$) inlet duct. This results in streamwise vortices impacting the fan at midspan.
- The in-duct acoustic effect of the vortex lift-off increases the propagated sound power from the inlet by 9 dB. This is due to reduced decay rates in the cut-off region near midspan caused by the increase in relative Mach number through the counter-swirling vortex.

While this work has focused on upstream-propagated tonal fan noise, this is only one of many engine noise sources. Extending the formulation of the body force blade row model to include the stator, the method is also suitable for studying rotor-stator interaction noise. There are two challenges that must be overcome to enable this additional capability: (1) obtaining accurate blade wakes using the body force approach and (2) modeling the blockage effect of the blade rows on noise.

Acknowledgment

The authors would like to thank Professor Nick Cumpsty for his helpful comments. This research was funded by the NASA Langley Research Center, Dr. Russell Thomas contract monitor.

Nomenclature

a = speed of sound
A = area, surface
AR = duct area ratio, A_{AIP}/A_{throat}
D = diameter
$DC(60)$ = distortion coefficient (worst 60 deg)
L = axial length of serpentine inlet
M = Mach number
OR = duct offset ratio, δ/D_{AIP}
p = static pressure
r = radial coordinate
r_c = radius of curvature
s^* = dimensionless arc length
u = velocity
x = axial coordinate
y = vertical coordinate
δ = duct vertical offset
Θ_{em} = acoustic emission angle
ρ = density
ω = angular frequency
Ω = fan rotational speed
AIP = aerodynamic interface plane
BLI = boundary-layer ingestion/ingesting
BPF = blade-passing frequency
FW-H = Ffowcs–Williams and Hawkings

B = blade row
M = mass-averaged
t = stagnation quantity
∞ = free-stream condition

References

[1] Mathews, D., and Nagel, R., 1973, "Inlet Geometry and Axial Mach Number Effects on Fan Noise Propagation," Aero-Acoustics Conference, Seattle, WA, October 15–19, AIAA Paper 1973-1022.

[2] Prasad, D., and Feng, J., 2005, "Propagation and Decay of Shock Waves in Turbofan Engine Inlets," ASME J. Turbomach., **127**(1), pp. 118–127.

[3] Plas, A., Sargeant, M., Madani, V., Chrichton, D., Greitzer, E., Hynes, T., and Hall, C., 2007, "Performance of a Boundary Layer Ingesting (BLI) Propulsion System," 45th American Institute of Aeronautics and Astronautics Aerospace Sciences Meeting and Exhibit, Reno, NV, January 8–11, AIAA Paper 2007-450.

[4] Madani, V., and Hynes, T., 2009, "Boundary Layer Ingesting Intakes: Design and Optimization," 19th International Society for Air Breathing Engines Conference, Montreal, Canada, September 13–18, ISABE Paper 2009-1346.

[5] Myers, M., 1991, "Transport of Energy by Disturbances in Arbitrary Steady Flows," J. Fluid Mech., **226**, pp. 383–400.

[6] Brambley, E., and Peake, N., 2007, "Sound in Curved Intakes," 13th AIAA/CEAS Aeroacoustics Conference, Rome, Italy, May 21–23, AIAA Paper 2007-3552.

[7] Brambley, E., and Peake, N., 2008, "Sound Transmission in Strongly Curved Slowly Varying Cylindrical Ducts With Flow," J. Fluid, **596**, pp. 387–412.

[8] Defoe, J., Narkaj, A., and Spakovszky, Z., 2010, "A Body-Force-Based Method for Prediction of Multiple-Pure-Tone Noise: Validation," Aero-Acoustics Conference, Stockholm, Sweden, June 7–9, AIAA Paper 2010-3747.

[9] Defoe, J., and Spakovszky, Z., 2013, "Shock Propagation and MPT Noise From a Transonic Rotor in Non-Uniform Flow," ASME J. Turbomach., **135**, p. 011016.

[10] Hughes, C., Jeracki, R., Woodward, R., and Miller, C., 2002, "Fan Noise Source Diagnostic Test—Rotor Alone Aerodynamic Performance Results," 8th AIAA/CEAS Aeroacoustics Conference and Exhibit, Breckenridge, CO, June 17–19, AIAA Paper 2002-2426.

[11] Hileman, J., Spakovszky, Z., and Drela, M., 2010, "Airframe Design for Silent Fuel-Efficient Aircraft," J. Aircraft, **47**(3), pp. 956–969.

[12] Defoe, J., Narkaj, A., and Spakovszky, Z., 2009, "A NovelMPT Noise Methodology for Highly-Integrated Propulsion Systems With Inlet Flow Distortion," 15th AIAA/CEAS Aeroacoustics Conference, May 11–13, AIAA Paper 2009-3366.

[13] Chen, X., Zhang, X., Morfey, C., and Nelson, P., 2004, "A Numerical Method for Computation of Sound Radiation From an Unflanged Duct," J. Sound Vib., **270**, pp. 573–586.

[14] Rumsey, C., Biedron, R., and Farassat, F., 1998, "Ducted-Fan Engine Acoustic Predictions Using a Navier–Stokes Code," J. Sound Vib., **213**(4), pp. 643–664.

[15] Huttl, T., Kahl, G., Kennepohl, F., and Heinig, K., 2001, "Resolution Requirements for the Numerical Computation of Tonal Noise in Compressors and Turbines of Aeroengines," NATO Research and Technology Organisation Applied Vehicle Technology Symposium on Ageing Mechanisms and Control: Part A—Developments in Computational Aero- and Hydro-Acoustics, Manchester, UK, October 8–11, RTO-MP-079(I).

[16] Greitzer, E., Tan, C., and Graf, M., 2004, *Internal Flow: Concepts and Applications*, Cambridge University Press, Cambridge, UK.